American Mineralogist, Volume 78, pages 941–951, 1993

Hematite-ilmenite (Fe_2O_3-$FeTiO_3$) solid solutions: Determinations of Fe-Ti order from magnetic properties

N. E. Brown,* A. Navrotsky
Department of Geological and Geophysical Sciences, Princeton University, Guyot Hall, Princeton, New Jersey 08544-1003, U.S.A.
G. L. Nord, Jr.
959 National Center, U.S. Geological Survey, Reston, Virginia 22092, U.S.A.
S. K. Banerjee
Department of Geology and Geophysics, University of Minnesota, 108 Pillsbury Hall, Minneapolis, Minnesota 55455, U.S.A.

Abstract

The saturation magnetization, $M_s(T)$, of samples with compositions spanning the ilmenite-hematite solid solution series has been measured at temperatures from 77 to 298 K. These data have been used to extrapolate to the saturation magnetization at 0 K. The saturation magnetization at 0 K is directly related to the distribution of Fe^{3+}, Fe^{2+}, and Ti^{4+} between the A and B sublattices of the ilmenite structure and can, therefore, be used to determine the order parameter, Q_{M_s}, for each composition and annealing temperature. Samples with compositions $x_{ilm} \geq 0.5$ (x_{ilm} = mole fraction ilmenite) have been annealed below the order-disorder transition and above the solvus (Burton and Davidson, 1988) to eliminate twin domain boundaries (TDBs) and prevent the development of compositional modulations. Both types of microstructures have been shown to affect the saturation magnetization (Nord and Lawson, 1992). For samples with $x_{ilm} = 0.6$, Q_{M_s} varies from 0 for samples quenched from 1573 K to 0.66 for samples annealed at 923 K. For samples with $x_{ilm} = 0.7$, Q_{M_s} varies from 0.53 for samples quenched from 1573 K to 0.66 for samples annealed at 1073 K. For samples with $x_{ilm} = 0.85$, no variation in Q_{M_s} occurs as a function of annealing temperature ($Q_{M_s} = 0.6$). The decreasing variation in Q_{M_s} with annealing temperature as compositions become more ilmenite rich may indicate that quenching the high-temperature disordered state becomes more difficult. For ilmenite, there appears to be no significant disorder. This implies that for samples with compositions between $x_{ilm} = 0.85$ and $x_{ilm} = 1.0$, the degree of order must abruptly increase.

High coercivities exhibited by samples with compositions $x_{ilm} = 0.6$ and $x_{ilm} = 0.7$ are related to the development of high TDB surface areas and short-range ordering, which result from quenching through the order-disorder transition. With subsequent annealing below the order-disorder transition, coercivities are drastically reduced. This decrease in coercivity is correlated with a significant decrease in TDB surface area. The higher coercivities associated with compositions of $x_{ilm} = 0.2$ and $x_{ilm} = 0.4$ suggest that these samples may also develop some short-range order upon quenching.

Introduction

Phases in the ilmenite-hematite series, $FeTiO_3$-Fe_2O_3, are the most important carriers after magnetite of thermoremanent magnetization (TRM) in natural materials. High coercivities and stable remanence make some members of the series important in paleomagnetic research.

The complex magnetic behavior in $FeTiO_3$-Fe_2O_3 phases has been studied by many workers (e.g., Bozorth et al., 1957; Ishikawa and Akimoto, 1957; Ishikawa, 1958b, 1962; Shirane et al., 1959, 1962; Ishikawa and Syono, 1963; Warner et al., 1972). These early papers reported that the magnetic properties of samples with compositions from $x_{ilm} = 0.4$ to $x_{ilm} = 0.75$ (x_{ilm} = mole fraction $FeTiO_3$) varied with the thermal history. Ordering of Fe and Ti between the A and B sublattices was interpreted to cause this variation. However, errors in determinations of composition (Nord and Lawson, 1989), limited control on the thermal histories of specimens with respect to the order-disorder transition and solvus (Nord and Lawson, 1992), and limited control of f_{O_2} prevented a clear assessment of the variation in magnetic properties as a function of cation ordering.

Later workers (Lawson et al., 1981; Nord and Lawson, 1988, 1989, 1992) have examined the relationship between magnetic properties and microstructures of samples with $x_{ilm} = 0.7$ that were synthesized at temperatures

* Present address: Bayerisches Geoinstitut, Universität Bayreuth, Postfach 10 12 51, D-95440 Bayreuth, Germany.

0003–004X/93/0910–0941$02.00

close to the order-disorder transition. These studies have provided visual evidence of the twin domain boundaries (TDBs) that arise from quenching through the order-disorder transition. In addition, these studies have demonstrated that the self-reversed TRM exhibited by compositions $0.45 \leq x_{ilm} \leq 0.75$ results from high TDB surface areas.

Structural background

The lattice of these phases is generally referred to with a triply primitive, hexagonal unit cell (in contrast to a primitive rhombohedral unit cell), with an almost hexagonally closest-packed array of O anions. Fe and Ti occupy the octahedral cation positions, as in the corundum structure. Each octahedron has one shared and one unshared face that are parallel to (0001). In the shared face, the O-O distance (2.669 Å in hematite) is close to that for ideal hexagonal closest-packing (HCP). In the unshared face, however, the O-O distance is greater (3.035 Å in hematite) than for ideal HCP (Lindsley, 1976a). This deviation from HCP produces a distortion of the octahedra in the structure. Electrostatic repulsion across the shared face causes a displacement of the cations toward the unshared face.

Hematite (Fe_2O_3) has the space group $R\bar{3}c$, whereas ilmenite ($FeTiO_3$) has the space group $R\bar{3}$ (a subgroup of $R\bar{3}c$) (Lindsley, 1976a). The loss of the c glide results from ordering of Fe and Ti on alternate planes parallel to (0001). Planes containing Fe make up the A sublattice, whereas those containing Ti make up the B sublattice.

Contrary to the work of Nagata and Akimoto (1956), Lindsley (1965) demonstrated that the unit-cell volume of Fe_2O_3-$FeTiO_3$ solid solutions did not vary linearly with composition. Since then, other workers have confirmed this nonlinear relationship (Hoffman, 1975; Nord and Lawson, 1989; this study). The compositional errors that plague the early work done on this system arise from their use of a linear volume vs. composition relationship. For intermediate compositions, this assumption can lead to errors that are as high as 7 mol% (Nord and Lawson, 1989).

Magnetic structure

Hematite is antiferromagnetic; within each (0001) plane, all Fe^{3+} moments are aligned parallel, whereas alternating (0001) planes of Fe^{3+} are oppositely magnetized. Imperfect antiferromagnetic coupling (Dzyaloshinsky, 1958) of the Fe^{3+} ions in the alternating A and B sublattices results in a small net ferromagnetic moment (parasitic ferromagnetism) in the (0001) plane. The magnetic interactions between Fe atoms on alternating sublattices are strong and are reflected in hematite's high Néel temperature, 950 K. Below 263 K (Morin transition), the antiferromagnetic ordering in hematite is parallel to the [0001] axis.

Ilmenite is also antiferromagnetic. The magnetic moments, however, are aligned parallel to the [0001] axis (Ishikawa et al., 1985). In ilmenite, the Fe^{2+} atoms are positioned in the A sublattices, and Ti atoms in the B sublattices. Hence, antiferromagnetic coupling occurs across two A layers separated by a B layer of Ti atoms (Shirane et al., 1959), and the magnetic unit-cell translation is double the crystallographic unit-cell translation in the [0001] direction. The magnetic interactions between Fe atoms on separate A sublattices are rather weak, as reflected in ilmenite's very low Néel temperature of 57 K (Shomate, 1946; Anovitz et al., 1985).

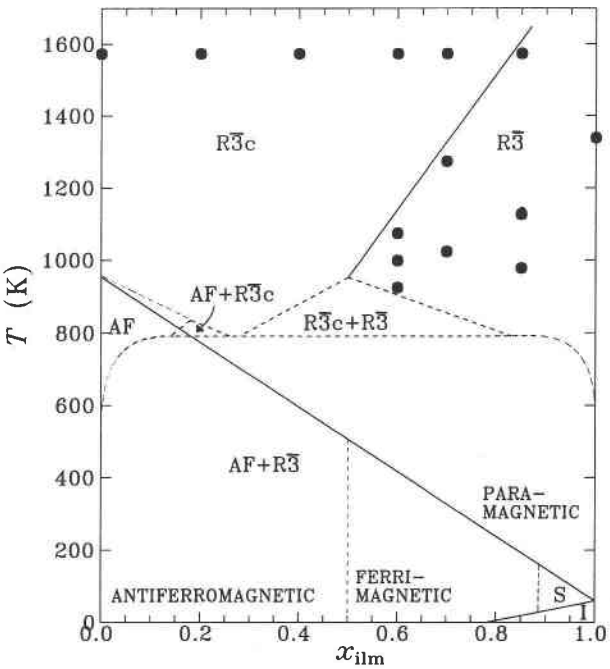

Fig. 1. Pseudobinary phase diagram of the hematite-ilmenite solid solution series (Burton and Davidson, 1988). Solid circles represent the temperatures and compositions of the solid solutions synthesized in this study. The long solid line indicates the variation in Néel temperature [i.e., the onset of antiferromagnetic ordering (AF)] with composition (Ishikawa and Akimoto, 1957). The region I, bounded by a solid line from $x_{ilm} = 0.79$ to $x_{ilm} = 1.00$, indicates materials with ilmenite-like antiferromagnetism (i.e., magnetic moments aligned parallel to the c axis) (Ishikawa, 1962). Ferrimagnetic ordering occurs for intermediate compositions and appears to be related to ordering of Fe and Ti on separate sublattices (Ishikawa, 1958b). The upper solid line from $x_{ilm} = 0.5$ to $x_{ilm} = 0.85$ represents the order-disorder transition (Nord and Lawson, 1989). The upper dashed lines are the two-phase regions and miscibility gap calculated by Burton and Davidson (1988).

For solid solutions intermediate in composition between hematite and ilmenite, the magnetic behavior becomes increasingly complicated as the compositions become more ilmenite rich. Below the Néel temperature, compositions $x_{ilm} \leq 0.5$ are antiferromagnetic (Fig. 1) with magnetic moments aligned as in hematite (Warner et al., 1972). Samples with these compositions also exhibit electron transfer between Fe^{2+} and Fe^{3+} that continues to occur in compositions up to $x_{ilm} = 0.6$ (Warner et al., 1972; Ishikawa, 1958a). Samples with compositions in

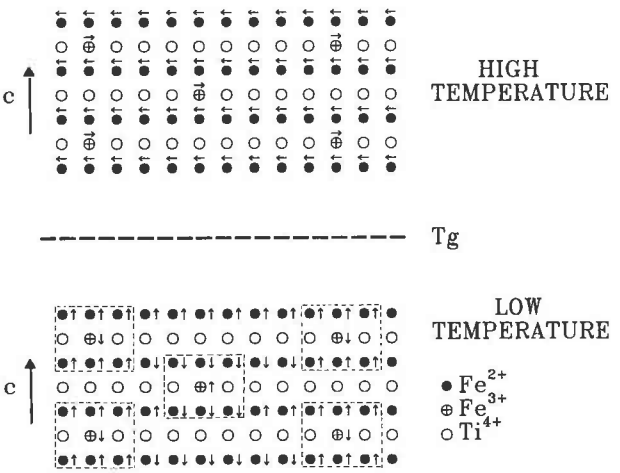

Fig. 2. Schematic representation, perpendicular to the c axis, of the magnetic ordering at temperatures above and below the spin glass transition, T_g, for compositions $x_{ilm} > 0.8$. The dashed lines bound the cluster areas of antiferromagnetic interactions between A and B sublattices (modified from Ishikawa et al., 1985). Small arrows indicate the alignment direction of magnetic moments. The large arrow indicates the c-axis direction.

the range $0.50 < x_{ilm} < 0.75$ are ferrimagnetic at room temperature (Fig. 1), with the net magnetic moments aligned parallel to the (0001) plane. For these compositions, the intensity of ferrimagnetism is strongly dependent on the thermal history of the sample (Ishikawa and Akimoto, 1957; Ishikawa, 1958b; Bozorth et al., 1957). The dependence of magnetic properties (e.g., Curie temperatures and saturation magnetization) on thermal history was interpreted to arise from changes in cation ordering. Because of poor control of sample thermal history, however, the behavior observed in these early studies was probably more complicated than this (Nord and Lawson, 1992). Nord and Lawson (1992) have shown that increases in Curie temperature also occur in samples that have been annealed within the solvus and exhibit weak compositional modulations. In addition, decreases in saturation magnetization values can also result from high surface area of TDBs.

For solid solutions $0.80 < x_{ilm} < 1$, the magnetic interactions are further complicated by the presence of a spin glass transition at low temperature (Ishikawa et al., 1983, 1985; Arai et al., 1985; Arai and Ishikawa, 1985). Above this transition (but below the Néel temperature), the solid solutions have magnetic moments aligned within the (0001) plane (Fig. 2; region S in Fig. 1). Below this transition, the alignment becomes parallel to the c axis (Fig. 2; region I in Fig. 1). The spin glass transition manifests itself as a maximum in the graph of magnetization vs. temperature (Ishikawa, 1962). Below the spin glass transition, however, the presence of Fe^{3+} in the structure produces small regions of antiferromagnetic coupling between A and B sublattices in a material having dominant antiferromagnetic coupling between A sublattices (Fig. 2). This produces a decrease in the magnetization at temperatures below the spin glass transition.

Ishikawa (1962) has shown that between the Néel temperature and the spin glass transition, samples with compositions $0.88 \leq x_{ilm} < 1$ are superparamagnetic (region S in Fig. 1), whereas those with compositions $x_{ilm} \leq 0.83$ exhibit both hysteresis and remanent magnetization. Hysteresis measurements made on samples with $x_{ilm} = 0.85$, however, also exhibit hysteresis at temperatures from 220 to 85 K (Fig. 3). We suggest, therefore, that the compositional limit should be extended to $x_{ilm} = 0.85$. This extension agrees with the data of Ishikawa (1962) when compositional corrections are applied.

Experimental procedures

The background information provided above has shown that for samples with $0.85 < x_{ilm} < 1.0$, magnetic properties cannot be used to determine the degree of order due to complex magnetic interactions. In addition, this information has demonstrated that determination of the degree of Fe-Ti order from the saturation magnetization requires that each sample has a well-defined thermal history. To eliminate variations in magnetic properties resulting from the presence of TDBs or compositional modulations, samples must be annealed at temperatures between the order-disorder transition and the solvus. Because of poor constraints on the position of the solvus (Lindsley, 1976b), annealing temperatures have been selected based on the calculated solvus of Burton and Davidson (1988). This calculated solvus encompasses the approximate position of the experimentally determined solvus of Lindsley (1976b).

Sample preparation

One-gram mechanical mixtures of dried reagent-grade TiO_2 and Fe_2O_3 were ground together for 1 h in an agate mortar. These mixtures were pressed into pellets of 100–300 mg placed on an Ag-Pd foil, and sintered at 1473 K in air. Following that, the pellets were wrapped in two loops of Pt wire 0.1 mm in diameter, suspended in a Deltech vertical tube furnace, and heated for 24 h at 1573 K. An H_2-CO_2 mixture was used to control the f_{O_2} of samples in the compositional range $x_{ilm} = 0.4$–0.85, whereas CO_2-O_2 was used to maintain the f_{O_2} for $x_{ilm} = 0.2$. Values of f_{O_2} were monitored using a ZrO_2-9 wt% Y_2O_3 ceramic electrolyte cell, with air as a reference (Huebner, 1987). Total flow rates of 100 cm³/min were maintained within 0.1% by means of mass flow regulators calibrated specifically for H_2, CO_2, and O_2. The open circuit cell emf was measured by means of an electrometer with an impedance of 10^{14} Ohm. This high impedance ensures that insignificant current flows through the electrolyte cell. A more in-depth discussion can be found in Huebner (1987). The cell was calibrated at 1573 K using the Ni-NiO O buffer. All samples were quenched by dropping them into H_2O; the quenching time was ~2 s. Ilmenite was synthesized from stoichiometric mechanical

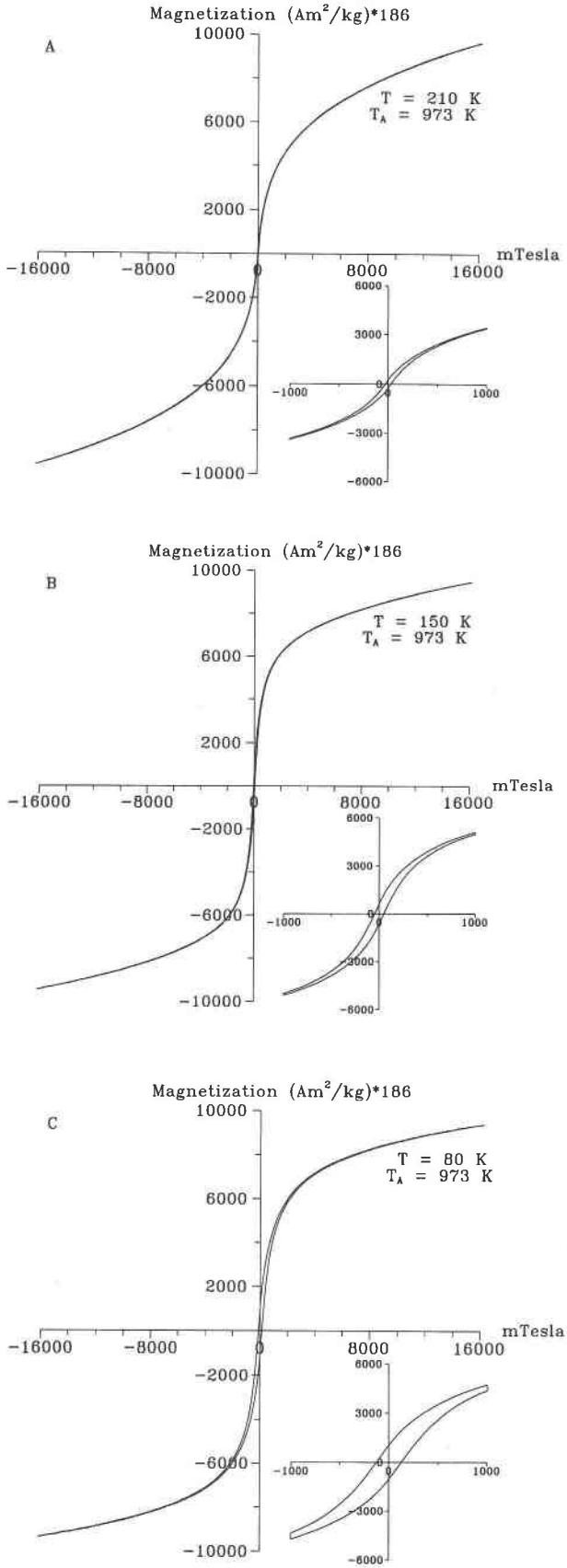

mixtures of reagent-grade Fe, Fe_2O_3, and TiO_2 by heating at 1338 K for 6 d in an evacuated silica tube.

Two stages of annealing were carried out in evacuated silica tubes within the single-phase $R\bar{3}$ stability field for compositions $x_{ilm} = 0.6$–0.85 (Fig. 1). Prior to annealing, each pellet was wrapped in Ag-Pd foil. The first stage involved heating for 15 h at temperatures ~50 K below the order-disorder transition. For samples with $x_{ilm} = 0.7$, Nord and Lawson (1989) have demonstrated that after this annealing procedure, the TDB surface area is greatly reduced and no longer affects the measured saturation magnetization. The second stage involved heating for 20 h at lower temperatures, to increase the degree of cation ordering.

Backscattered imaging of initial 1273-K annealing experiments revealed oxidation rims of an $FeTi_2O_5$-Fe_2TiO_5 phase on ilmenite grains within the pellet. These rims were not visible by reflected light microscopy because they were obscured by the grain boundaries. In only one annealing experiment, in which the pellet contained <1% Fe_3O_4-Fe_2TiO_4, were these oxidation rims not observed by backscattered imaging. As a result of this observation, each stage of annealing (discussed above) contained two pellets: one single-phase pellet of the desired composition and an additional pellet of the same composition but containing ~1% Fe_3O_4-Fe_2TiO_4. The latter pellet was synthesized at 1573 K with log f_{O_2} from 0.1 to 0.2 log units more reducing than that for the single-phase pellet of the same composition. This pellet buffered each annealing experiment at the f_{O_2} necessary to maintain a single phase hematite-ilmenite solid solution. Backscattered imaging of annealing experiments carried out in this manner revealed no oxidation rims.

Microprobe analyses

Chemical compositions of each synthesized sample were determined by electron microprobe analyses on a Jeol JXA-8600 Superprobe at Rutgers University. The microprobe was operated at 15 keV, with a 15-nA beam current and a 1-μm beam diameter. Counting proceeded for 20 s or until <1% sd in the counting statistics was achieved. Grain sizes ranged from ~30 μm for hematite to ~100 μm for $x_{ilm} = 0.85$. For compositions, $x_{ilm} \geq 0.6$, ilmenite was used to calibrate both Fe and Ti. For compositions $x_{ilm} \leq 0.4$, magnetite was used to calibrate Fe and ilmenite was used to calibrate Ti. Data reduction followed the procedures for ZAF corrections (Vaughan, 1983). Twenty to 25 spot analyses were made on the grains from each

←

Fig. 3. Hysteresis behavior at 210 K (**A**), 150 K (**B**), and 80 K (**C**), for $x_{ilm} = 0.85$, with a maximum applied field of 1.6 T. The small inserts show the hysteresis data for field strengths up to 0.1 T. Hysteresis is observed at all temperatures, indicating no superparamagnetic behavior. T_A is the annealing temperature of the sample.

experiment. Compositions were calculated assuming stoichiometry and are listed in Table 1.

Backscattered electron imaging showed experimental products to be homogeneous and single phase at the resolution of the microprobe (1 μm), except where indicated in Table 1. For samples in which a second phase was detected by backscattered electron imaging, 600 spots were analyzed to estimate its content. Additionally, qualitative EDS spectra were acquired to determine whether the second phase was an Fe_2TiO_5-$FeTi_2O_5$ or an Fe_3O_4-Fe_2TiO_4 solid solution. In all cases, the second phase (if present) made up <0.7% of the sample and occurred in equant grains, rather than as oxidation-exsolution lamellae.

Qualitative energy-dispersive analyses did not reveal the presence of any compositional impurities (e.g., Pt, Al, or Si) in the experimental products.

X-ray diffraction studies

Room-temperature X-ray diffraction patterns were obtained with a Scintag PAD V X-ray powder diffractometer equipped with a solid-state detector and Cu$K\alpha$ radiation. Si was used as an internal standard, and scan rates were 0.3° 2θ/min. Each sample was scanned three times, and all data were used in the least-squares refinement of lattice parameters (Appleman and Evans, 1973). Eight to 15 reflections from each scan over a 2θ range from 20 to 90° were used in the refinements.

Magnetic studies

Magnetic hysteresis measurements were carried out on a PAR model 155 vibrating sample magnetometer in the Rock Magnetism Laboratory at the University of Minnesota. Three measurements were obtained for each sample at temperatures from 79 to 298 K, except for x_{ilm} = 0.85, for which the highest temperature was 210 K. Temperatures were maintained by means of a DRC-80C temperature controller within an accuracy of 0.5 K. The maximum applied field was 1.6 Tesla. The magnetometer was calibrated with Ni metal.

TABLE 1. Sample compositions determined by microprobe analyses and the order parameter, Q_{M_s}, determined from the saturation magnetization at 0 K

T (K)	No. of phases (percent second phase)*	Mole fraction $FeTiO_3$**	Order parameter (Q_{M_s})†
1573	1	0	—
1573	2 (0.7% FPB)	0.1946(70)	0
1573	1	0.2024(30)	0
1573	1	0.4080(2)	0
1573	1	0.4055(22)	0
1573	2 (0.1% MAG)	0.6094(14)	0.01(3)
1073	2 (0.1% MAG)	0.5993(24)	0.36(3)
998	1	0.6013(18)	0.55(3)
923	1	0.5929(30)	0.66(3)
1573	2 (0.1% MAG)	0.6969(14)	0.54(3)
1573	1	0.6969(3)	0.54(3)
1573	1	0.7001(29)	0.53(3)
1273	1	0.7023(7)	0.64(3)
1023	1	0.7029(7)	0.66(3)
1573	2 (0.1% FPB)	0.8621(20)	0.62(3)
1573	2 (0.1% FPB)	0.8630(11)	0.62(3)
1126	1	0.8570(7)	0.58(3)
977	1	0.8595(4)	0.61(3)

* The percent second phase has been determined by counting 600 points per sample in a backscattered electron imaging mode on a Jeol 8600 microprobe, in conjunction with qualitative EDS analysis to determine the composition of the second phase. The abbreviation FPB indicates that the second phase is an Fe_2TiO_5-$FeTi_2O_5$ solid solution. The abbreviation MAG indicates the second phase is an Fe_3O_4-Fe_2TiO_4 solid solution.

** Numbers in parentheses represent the precision of the microprobe measurements, as determined from the 2σ of the mean error in weight percent FeO and TiO_2, on the assumption of stoichiometry.

† Defined as $Q_{M_s} = M_s(0)/M_0$ (see text for definitions). Numbers in parentheses represent the estimated error in the order parameter, calculated on the basis of an error in Ti site occupancy of ±0.17. See note in Table 3.

THE ORDER PARAMETER, Q_{M_s}

The macroscopic order parameter is directly related to structural conditions on a microscopic scale. In the $R\bar{3}c$-$R\bar{3}$ order-disorder transition the order parameter determined from saturation magnetization measurements, Q_{M_s}, varies directly with the crystallographic site occupancies of Ti^{4+}, Fe^{3+}, and Fe^{2+}. In the general case, the three cations would be distributed over the A and B sublattices such that charge balance over the structure would be maintained and cation to cation repulsion across the shared octahedral face would be minimized. Cation to cation repulsive forces across the shared octahedral face can be expected to increase in the following order: Fe^{2+}-Fe^{2+} < Fe^{2+}-Fe^{3+} < Fe^{3+}-Fe^{3+} < Fe^{2+}-Ti^{4+} < Fe^{3+}-Ti^{4+} < Ti^{4+}-Ti^{4+}. One might assume that by maximizing Fe^{2+}-Fe^{2+} and Fe^{2+}-Fe^{3+} pairs a desirable configuration would be created. Such configurations, however, also increase the number of highly repulsive Ti^{4+}-Ti^{4+} pairs, particularly for ilmenite-rich compositions. Minimization of Ti^{4+}-Ti^{4+} pairs in both ordered and disordered solid solutions of all compositions occurs when Fe^{3+} is distributed equally in the A and B sites. Such a configuration is also consistent with pairwise electron transfer between Fe^{2+} and Fe^{3+} on the A and B sublattices in disordered solid solutions with $x_{ilm} \leq 0.6$ (Warner et al., 1972). Assuming that Fe^{3+} is equally distributed over both sublattices, therefore, we need only be concerned with the ordering of Fe^{2+} and Ti^{4+} on the A and B sublattices. The order parameter, Q_{M_s}, is related to the site occupancies by the general definition

$$Q_{M_s} = (X_{Fe^{2+},A} - X_{Fe^{2+},B})/(X_{Fe^{2+},A} + X_{Fe^{2+},B})$$
$$= (X_{Ti^{4+},A} - X_{Ti^{4+},B})/(X_{Ti^{4+},A} + X_{Ti^{4+},B}) \quad (1)$$

where $X_{Fe^{2+},A}$ is the sublattice mole fraction of Fe^{2+} in the A sublattice.

Inasmuch as the A and B crystallographic sublattices are identical to the A and B magnetic sublattices, the saturation magnetization at 0 K [$M_s(0)$] can be used to determine the degree of order. $M_s(0)$ is the sum of the magnetic moments of all the ions in the A sublattice minus the sum of the magnetic moments of all the ions in the B sublattice

$$M_s(0) = (5X_{Fe^{3+},A} + 4X_{Fe^{2+},A}) - (5X_{Fe^{3+},B} + 4X_{Fe^{2+},B}) \quad (2)$$

TABLE 2. Lattice parameters of synthetic hematite-ilmenite solid solutions

Mole fraction $FeTiO_3$	T (K)	a (Å)	c (Å)	V (Å^3)
0	1573	5.0356(3)	13.747(2)	301.88(4)
0.1946	1573	5.0428(3)	13.797(1)	303.85(4)
0.2024	1573	5.0444(4)	13.798(2)	304.06(4)
0.4080	1573	5.0552(4)	13.853(2)	306.59(5)
0.4055	1573	5.0532(4)	13.849(1)	306.25(4)
0.6094	1573	5.0684(3)	13.9151(9)	309.57(3)
0.5993	1073	5.0684(2)	13.9148(8)	309.55(3)
0.6013	998	5.0695(5)	13.910(2)	309.60(6)
0.5929	923	5.0689(3)	13.9145(8)	309.61(3)
0.6969	1573	5.0703(6)	13.944(4)	310.45(9)
0.6969	1573	5.0715(4)	13.950(1)	310.72(5)
0.7001	1573	5.0715(3)	13.9549(9)	310.72(4)
0.7023	1273	5.0735(4)	13.953(1)	311.04(4)
0.7029	1023	5.0750(3)	13.951(1)	311.17(3)
0.8621	1573	5.0813(5)	14.017(2)	313.19(6)
0.8630	1573	5.0798(4)	14.007(1)	313.02(5)
0.8570	1023	5.0820(4)	14.013(1)	313.43(5)
0.8595	973	5.0820(4)	14.009(2)	313.33(5)
0.9998	1338	5.0881(3)	14.082(1)	315.72(5)

Note: numbers in parentheses represent the standard deviation of the least-squares fit in the last decimal place.

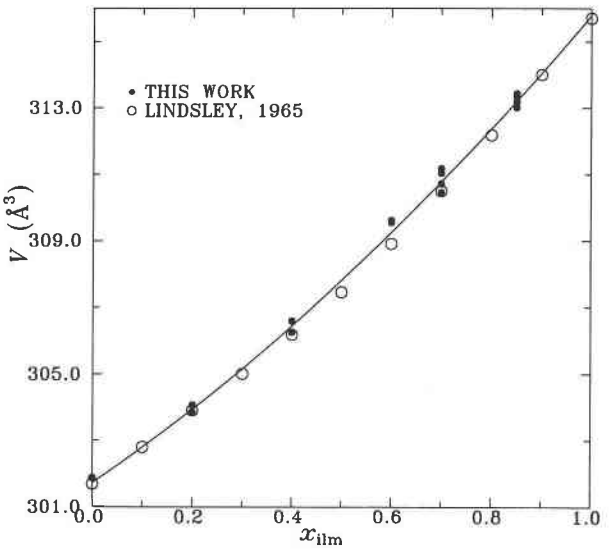

Fig. 4. Variation in unit-cell volume with composition. The solid circles represent our data; the open circles are from Lindsley (1965). The symbol size represents the error in the data. Larger errors have been attributed to Lindsley's data because the values have been estimated from graphical representation. The curve represents the least-squares regression of both data sets.

where the maximum magnetic moment per ion of Fe^{3+} and Fe^{2+} is 5 and 4 Bohr magnetons, respectively. This relationship assumes that the magnetic moments are collinear. The total moment of the B sublattice is subtracted from that of the A sublattice because of the ferrimagnetic structure where the spins of the A sublattice (M_A) are antiparallel to the spins of the B sublattice (M_B). M_A is > M_B because Fe^{2+} preferentially orders into A.

With the assumption that $X_{Fe^{3+},A} = X_{Fe^{3+},B}$ (see discussion above),

$$M_s(0) = 4(X_{Fe^{2+},A} - X_{Fe^{2+},B}). \quad (3)$$

The saturation magnetization of the fully ordered phase, M_0, is

$$M_0 = 4X_{Fe^{2+},A} = 4x_{ilm} = 4(X_{Fe^{2+},A} - X_{Fe^{2+},B}). \quad (4)$$

Therefore, M_0 ranges from 4 Bohr magnetons pfu for pure ilmenite to 0 Bohr magnetons pfu for pure hematite, if it is assumed that the entire solid-solution series has the same magnetic structure. The order parameter is calculated by relating $M_s(0)$ to the theoretical saturation of the fully ordered phase at 0 K (M_0),

$$Q_{M_s} = M_s(0)/M_0. \quad (5)$$

Inasmuch as $M_s(0)$ is measured in ampere meters squared per kilogram and M_0 in Bohr magnetons per formula unit, $M_s(0)$ can be converted into the same units as M_0 by the relation

$$M_s(0) \text{ (Bohr magnetons pfu)} = M_s(0)(\text{Am}^2/\text{kg})W/\mu_B N_A \quad (6)$$

where W is the molecular weight in kilograms per mole; μ_B is the Bohr magneton number = $9.2740154 \times 10^{-24}$ (Cohen and Taylor, 1990); and N_A is Avogadro's number.

RESULTS

Compositional determination

The chemical composition of each synthesized phase was determined by three methods: wavelength-dispersive microprobe analysis (WDS), X-ray powder diffraction, and wet chemical analysis. Lattice-parameter measurements and wet chemical analyses were completed to corroborate the microprobe analyses, which were calculated on the basis of 3 O apfu. The use of three independent techniques also serves to reveal the true compositional variability for each phase, which exceeds the compositional precision of the microprobe analyses.

Lattice parameters determined by X-ray analysis on samples from this study are listed in Table 2. In Figure 4, unit-cell volumes are compared with those of Lindsley (1965). The results agree well with Lindsley's data. Volume data can, therefore, be used to determine the compositions of the synthesized phases, providing an independent check on the microprobe analyses. Compositions determined by the microprobe and those from lattice parameters are in good agreement (Fig. 5). These results, however, do not test the assumption of stoichiometry in the microprobe analyses. For this reason, further wet chemical analyses were completed on each composition, following the procedures of Fritz and Popp (1985). These results are also shown in comparison with the microprobe analyses in Figure 5. The overall results, which are quite consistent, allow us to conclude that the overall compositional uncertainty is $\sim \pm 1$ mol%.

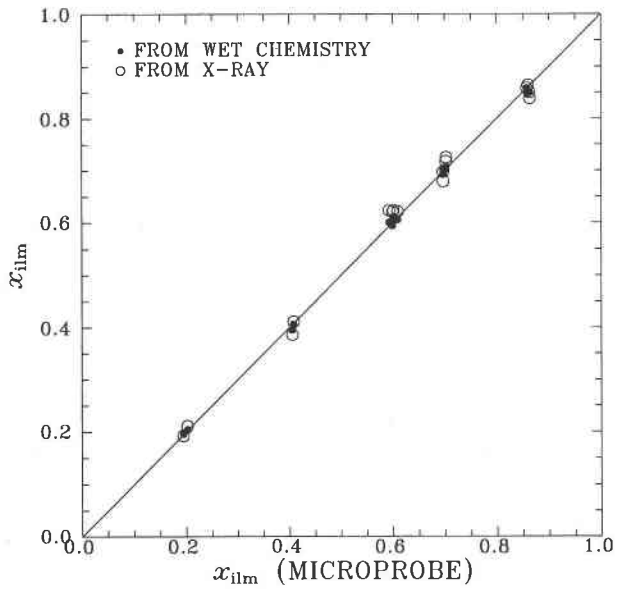

Fig. 5. Mole fraction $FeTiO_3$ determined from microprobe analyses vs. that determined from X-ray powder diffraction measurements of the unit-cell volume (open circles) and wet chemical analyses of Fe^{2+}, Fe_{tot}, and Ti (solid circles). The line represents a 1:1 compositional correlation.

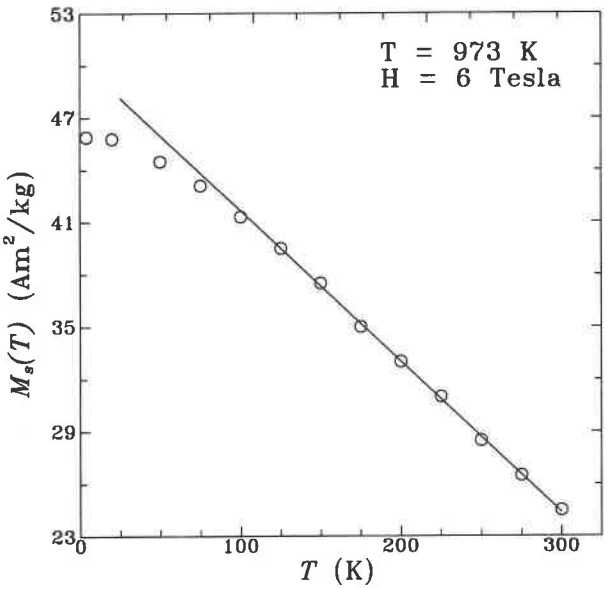

Fig. 6. Saturation magnetization (squared ampere meters per kilogram), $M_s(T)$, vs. temperature for samples with $x_{ilm} = 0.6$, quenched from 973 K (Nord, in preparation). $M_s(T)$ was determined by hysteresis measurements made with a maximum applied field strength (H) of 6 T. The quantum mechanical effects, which cause $dM_s(T)/dT$ to approach zero as T approaches zero (Salje et al., 1991), are clearly shown by the change in slope of the data at low temperatures. $M_s(T)$ begins to level off at $T \leq 100$ K and causes a systematic underestimation of the saturation magnetization at 0 K.

Saturation magnetization

The measured saturation magnetization, $M_s(T)$, was determined at temperatures from 77 to 298 K, by fitting the hysteresis data to the empirical relationship

$$M_H = M_s(T)[1 - a/H - b/H^2] + cH \quad (7)$$

where M_H is the measured magnetization in the field H and a, b, and c are constants. This relationship has been shown to describe many ferromagnetic materials for applied fields from 0.1 to 3 T (Morrish, 1965). Values of $M_s(0)$ were determined by the linear extrapolation to 0 K of the slope of the $M_s(T)$ vs. T data obtained at $T >$ 150 °C. This procedure was followed to avoid the quantum mechanical effects that cause $dM_s(T)/dT$ to approach 0 as T approaches 0 K (Salje et al., 1991). These effects are illustrated by an independent set of magnetic measurements that show the saturation magnetization [$M_s(T)$] as a function of temperature for $x_{ilm} = 0.6$ quenched from 973 K (Nord, unpublished data; Fig. 6). The leveling off of $M_s(T)$ begins to take effect at $T \leq 100$ K and causes a systematic underestimation of the saturation magnetization at 0 K. Agreement between the hysteresis data acquired at maximum field strengths of 1.6 and 6 T show that Equation 7 can be reliably used to determine $M_s(T)$ even at the lower field strength.

Values of $M_s(T)$ for each annealing temperature are shown in Figure 7A, 7B, and 7C for compositions $x_{ilm} = 0.6$, $x_{ilm} = 0.7$, and $x_{ilm} = 0.85$, respectively. The linear variation in $M_s(T)$ vs. temperature at $T > 150$ K agrees well with the experiments of Ishikawa and Akimoto (1957). Absolute values for $M_s(T)$ at room temperature and extrapolated values at 0 K also agree well with those of Ishikawa and Akimoto (1957) and Ishikawa (1958b), if compositional corrections are made to their data (Nord and Lawson, 1989).

For samples with composition $x_{ilm} = 0.85$, all hysteresis measurements were made above the glass transition temperature, $T_g \simeq 20$ K (estimated from Ishikawa, 1962), but below the Néel temperature (~220 K), in the temperature range in which the magnetic moments are aligned parallel to (0001) (Ishikawa et al., 1983) (Fig. 2). Thus, the extrapolated values of $M_s(0)$ represent theoretical values based on the assumption that the moments are all of this character. Our data for $x_{ilm} = 0.85$ and those of Ishikawa and Akimoto (1957) and Ishikawa (1958b) exhibit differences because they obtained saturation values measured below the spin glass transition. The use of $M_s(T)$ values measured below the spin glass transition to determine the degree of cation order is dubious because Equations 2 and 3 no longer apply to the bulk material (Fig. 2).

Figure 8 shows the order parameter for each composition and annealing temperature vs. mole fraction of $FeTiO_3$. A value of $Q_{M_s} = 0$ indicates complete disorder, whereas a value of $Q_{M_s} = 1.0$ indicates complete order. The data suggest that, for $x_{ilm} = 0.2$, $x_{ilm} = 0.4$, and $x_{ilm} = 0.6$ quenched from 1573 K, the samples are completely

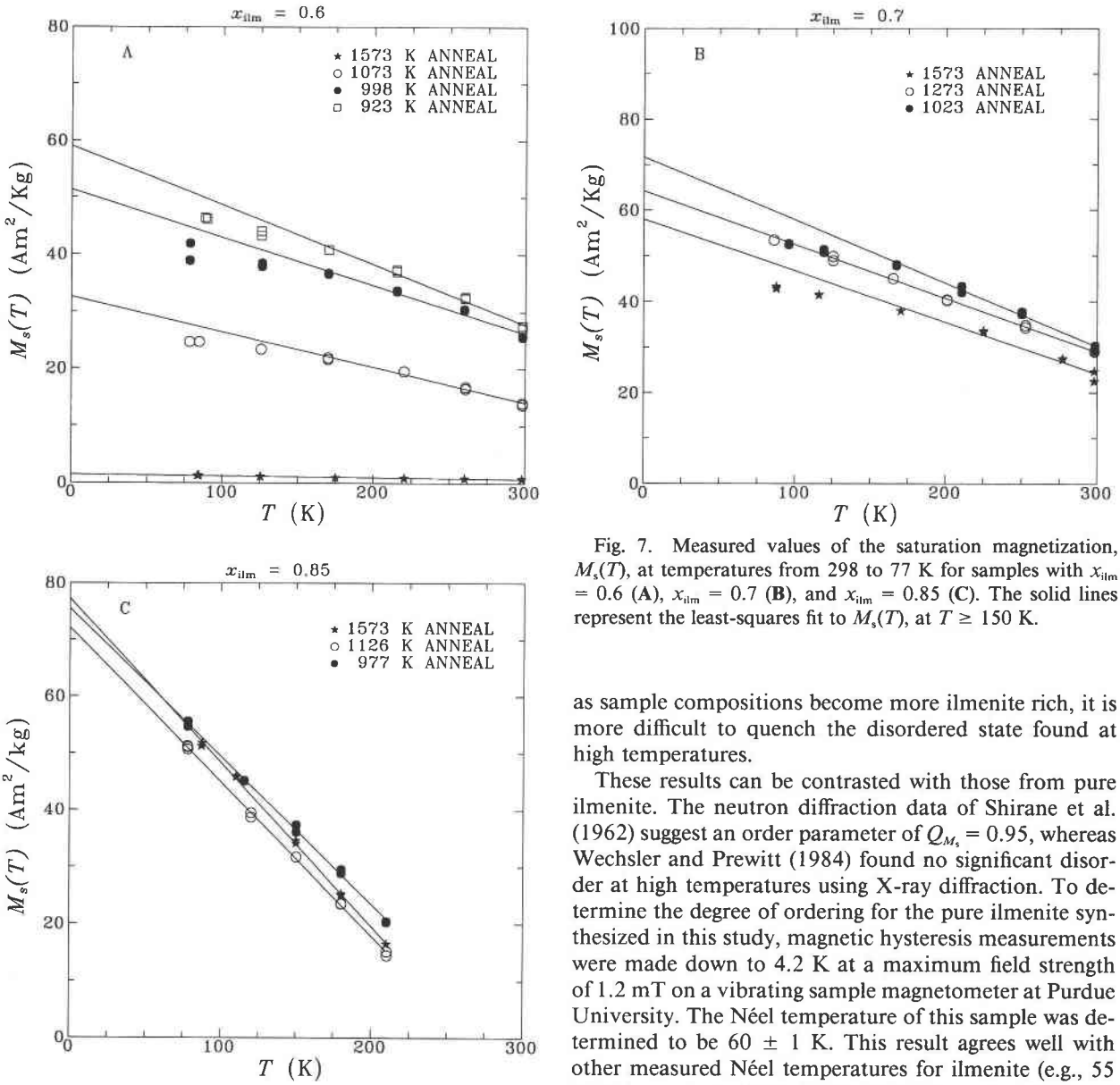

Fig. 7. Measured values of the saturation magnetization, $M_s(T)$, at temperatures from 298 to 77 K for samples with x_{ilm} = 0.6 (**A**), x_{ilm} = 0.7 (**B**), and x_{ilm} = 0.85 (**C**). The solid lines represent the least-squares fit to $M_s(T)$, at $T \geq 150$ K.

disordered. When samples with x_{ilm} = 0.6 are annealed at temperatures below the order-disorder transition, they become gradually more ordered with decreasing annealing temperature, reaching Q_{M_s} = 0.66 at 923 K (Table 3, Figs. 7A, 8). Similar behavior is exhibited by samples with x_{ilm} = 0.7 (Table 3, Figs. 7B, 8). However, the range in the degree of ordering is generally less, varying from Q_{M_s} = 0.53 at 1573 K to 0.66 at 1073 K. For samples with x_{ilm} = 0.85, there is no variation in the degree of order as a function of annealing temperatures; in all cases Q_{M_s} = 0.60 ± 0.02 (Table 3, Figs. 7C, 8). The systematic decrease in the variation of the order parameter with annealing temperature has also been reported by other workers (Bozorth et al., 1957; Ishikawa and Akimoto, 1957; Ishikawa, 1958b). This decrease may indicate that, as sample compositions become more ilmenite rich, it is more difficult to quench the disordered state found at high temperatures.

These results can be contrasted with those from pure ilmenite. The neutron diffraction data of Shirane et al. (1962) suggest an order parameter of Q_{M_s} = 0.95, whereas Wechsler and Prewitt (1984) found no significant disorder at high temperatures using X-ray diffraction. To determine the degree of ordering for the pure ilmenite synthesized in this study, magnetic hysteresis measurements were made down to 4.2 K at a maximum field strength of 1.2 mT on a vibrating sample magnetometer at Purdue University. The Néel temperature of this sample was determined to be 60 ± 1 K. This result agrees well with other measured Néel temperatures for ilmenite (e.g., 55 K: Shirane et al., 1959, 1962; 57 K: Shomate, 1946, and Anovitz et al., 1985; 68 K: Bizette and Tsai, 1956). The results from the hysteresis experiments yield a value for the saturation magnetization at 0 K of 0 Am²/kg. This value is that expected for a completely ordered ilmenite with antiferromagnetic-magnetic alignment between Fe^{2+} ions on alternating A sublattices. The fact that ilmenite is nearly or completely ordered indicates that, in the compositional range $0.85 < x_{ilm} < 1$, the order parameter must increase abruptly.

Coercivity

The coercivity of a material denotes the strength of the magnetic field required to reduce its magnetization from that at saturation to zero. The effects of composition and heat treatment on the coercivity of compositions across the hematite-ilmenite solid solution series is remarkable.

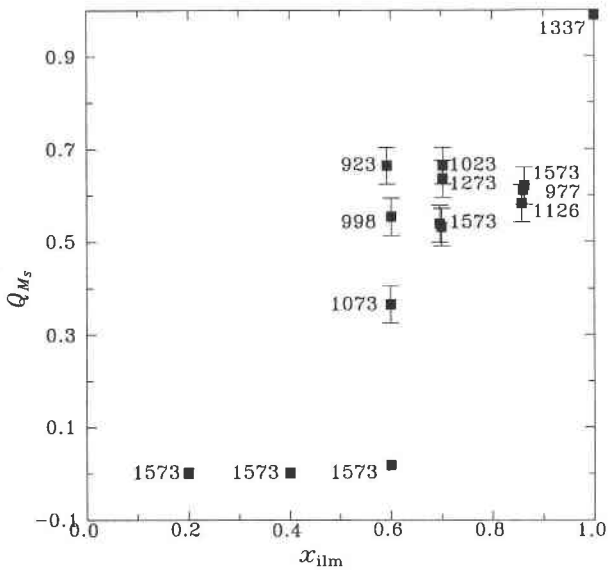

Fig. 8. Values of the order parameter, Q_{M_s} vs. composition where $Q_{M_s} = M_s(0)/M_0$, as described in text. The error bars represent the uncertainties arising from errors in site occupancies (see Table 3). The numbers by each symbol represent the annealing temperatures.

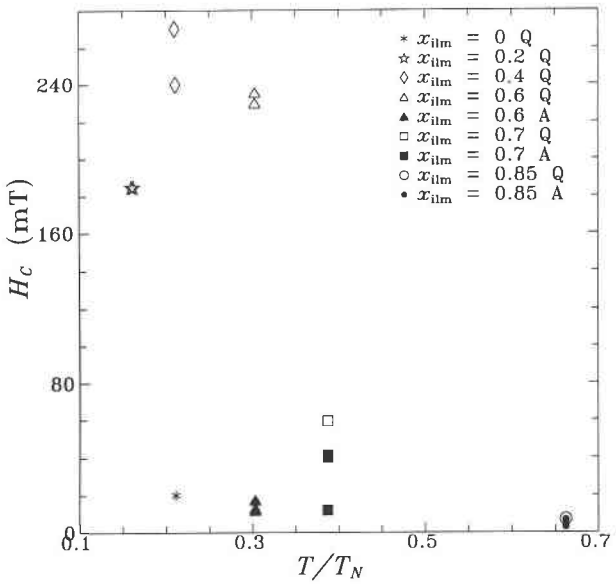

Fig. 9. The coercivity, H_c, for each solid solution is plotted vs. normalized temperature (T/T_N); T_N is the Néel temperature of each solid solution. The temperature during measurement, T, is 125 K, except for $x_{ilm} = 0$, for which the lowest measurement temperature was 200 K. Samples quenched from 1573 K are indicated by (Q), and those that have been annealed below the order-disorder transition by (A).

Nagata and Akimoto (1956) originally described a maximum in coercivity at $x_{ilm} = 0.2$. This maximum was later attributed to magnetostrictive strain arising from microscopic exsolution of ilmenite-rich lamellae in the hematite-rich host (Merrill, 1968). In natural hematite-ilmenite solid solutions, common sources for high coercivities are small grain sizes (i.e., single domain grains; Thompson and Oldfield, 1986) and exsolution (Merrill, 1968) that result from chemical alteration over long periods of time. However, a strong variation in the coercivity of the lamellae-free, multidomain materials synthesized in our study is also evident (Fig. 9). The most interesting aspect of this variation is the difference in coercivity between quenched and annealed samples (Fig. 9).

Samples with compositions $x_{ilm} = 0.6$ and $x_{ilm} = 0.7$ (Fig. 10A, 10B) quenched from 1573 K show significantly higher coercivities than those samples annealed at temperatures below the order-disorder transition. This behavior can be correlated with the development of twin domain boundaries during quenching from high temper-

TABLE 3. Site occupancy data and values of the saturation magnetization at 0 K for each composition and annealing temperature

Annealing T (K)	Mole fraction $FeTiO_3$	$X_{Ti^{4+},B}$*	$X_{Fe^{2+},B}$**	$X_{Fe^{3+},B}$†	$X_{Ti^{4+},A}$**	$X_{Fe^{2+},A}$*	$X_{Fe^{3+},A}$†	Saturation magnetization (μ_B/molecule)	Saturation magnetization (Am²/kg)
1573	0.8621	0.698	0.166	0.137	0.166	0.698	0.137	2.11	77.27
1126	0.8570	0.677	0.180	0.143	0.180	0.677	0.143	1.98	72.17
977	0.8595	0.691	0.169	0.140	0.169	0.691	0.140	2.08	75.83
1573	0.6969	0.548	0.148	0.303	0.148	0.548	0.303	1.60	58.00
1273	0.7023	0.572	0.130	0.298	0.130	0.572	0.298	1.77	64.20
1023	0.7029	0.599	0.104	0.297	0.104	0.599	0.297	1.98	71.70
1573	0.6094	0.311	0.299	0.391	0.299	0.311	0.391	0.04	1.46
1073	0.5993	0.414	0.186	0.401	0.186	0.414	0.401	0.91	32.60
998	0.6013	0.480	0.122	0.399	0.122	0.480	0.399	1.43	51.30
923	0.5929	0.502	0.091	0.407	0.091	0.502	0.407	1.64	59.00
1573	0.4055	0.206	0.202	0.593	0.202	0.206	0.593	0.002	0.08
1573	0.2024	0.102	0.097	0.802	0.097	0.102	0.802	0.003	0.12

Note: $X_{Ti^{4+},B}$ and $X_{Ti^{4+},A}$ are the sublattice mole fractions of Ti^{4+} in the B and A sublattices, respectively. Errors in site occupancies range from 0.01 to 0.024. They have been determined by including the errors arising from the linear extrapolations of the $M_s(T)$ vs. T data to 0 K and the 1-mol% errors in composition. See text for conversion of saturation magnetization units from ampere meters squared per kilogram to Bohr magnetons per molecule.

* $X_{Ti^{4+},B} = X_{Fe^{2+},A} = [x_{ilm}(1 + Q_{M_s})]/2$ (refer to text for definition of Q_{M_s}).

** $X_{Fe^{2+},B} = X_{Ti^{4+},A} = [x_{ilm}(1 - Q_{M_s})]/2$ (refer to text for definition of Q_{M_s}).

† $X_{Fe^{3+},A} = X_{Fe^{3+},B} = (1 - x_{ilm})$.

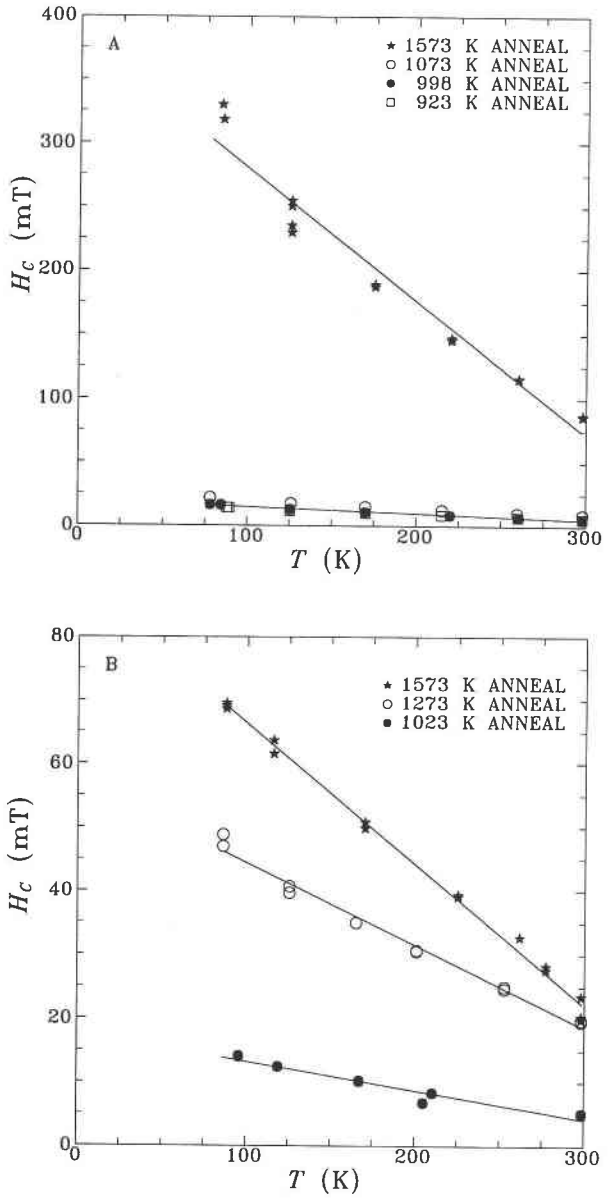

Fig. 10. (**A**) The coercivity, H_c, of samples with $x_{ilm} = 0.6$, measured at temperatures between 298 and 77 K. Also shown are the annealing temperatures of individual samples. Lines represent the least-squares fit to the data. (**B**) The coercivity, H_c, of $x_{ilm} = 0.7$ measured at temperatures between 298 and 77 K.

ature (Lawson et al., 1981; Nord and Lawson, 1988, 1989, 1992). In addition, samples with $x_{ilm} = 0.7$ exhibit a systematic increase in resistance to alternating-field demagnetization with increasing concentration of TDBs (Nord and Lawson, 1992). Annealing below the transition temperature results in a substantial decrease of TDBs (Lawson et al., 1981; Nord and Lawson, 1988, 1989, 1992) and a drastic reduction in the coercivity of the materials (Figs. 9, 10A, and 10B). The data support the suggestion of Nord and Lawson (1992) that these TDBs act as defect sites at which the magnetic domain walls become pinned. For annealed samples in which the number of twin domain boundaries does not change, the difference in the coercivities is negligible (Fig. 10A). These results suggest that the high coercivities associated with quenched samples with compositions $x_{ilm} = 0.6$ and $x_{ilm} = 0.7$ result from the development of TDBs and the accompanying short-range chemical order during quenching through the order-disorder transition.

The variation in coercivities with composition is also quite interesting. As the normalized temperature, T/T_N, approaches 1.0, the coercivity is expected to decrease considerably. This overall trend can be observed in Figure 9. However, it is interesting to note that the coercivities of samples with compositions $x_{ilm} = 0.4$ and $x_{ilm} = 0.2$ are significantly higher than for hematite. This result is contrary to what one would expect to see based on their Néel temperatures. This result also cannot be explained by variations in thermal history because all compositions have been synthesized at the same temperature and quenched in the same manner. Possible explanations for these high coercivities are the development of short-range ordering or chemical clustering during quenching.

Acknowledgments

Funding for this research was provided by the Mineralogical Society of America through its 1989 Petrology Grant (to N.E.B.) and by the National Science Foundation grant number DMR-89-12549 (to A.N.). The authors would also like to thank Maria Borscik for making the wet chemical analyses, Zbigniew Kakol for magnetically analyzing ilmenite at Purdue University, and Dong-ning Zheng for making 6-T magnetic hysteresis measurements (for a sample with $x_{ilm} = 0.6$) at the Superconductivity Research Centre, Cambridge University. The authors are grateful for the constructive reviews of the manuscript given by E. Larson, D. Sherman, J.S. Huebner, and R.A. Robie.

References cited

Anovitz, L.M., Treiman, A.H., Essene, E.J., Hemingway, B.S., Westrum, E.F., Wall, V.J., Burriel, R., and Bohlen, S.R. (1985) The heat-capacity of ilmenite and phase equilibria in the system Fe-Ti-O. Geochimica et Cosmochimica Acta, 49, 2027–2040.

Appleman, D.E., and Evans, H.T. (1973) Job 9214: Indexing and least-squares refinement of powder diffraction data. U.S. National Technical Information Service, Document PB 216 188.

Arai, M., and Ishikawa, Y. (1985) A new oxide spin glass system of $(1 - x)FeTiO_3$-xFe_2O_3. III. Neutron scattering studies of magnetization processes in a cluster type spin glass of $90FeTiO_3$-$10Fe_2O_3$. Journal of the Physical Society of Japan, 54, 795–802.

Arai, M., Ishikawa, Y., Saito, N., and Takei, H. (1985) A new oxide spin glass system of $(1 - x)FeTiO_3$-xFe_2O_3. II. Neutron scattering studies of a cluster type spin glass of $90FeTiO_3$-$10Fe_2O_3$. Journal of the Physical Society of Japan, 54, 781–794.

Bizette, H., and Tsai, B. (1956) Susceptibilités magnétique principales d'un cristal natural d'ilmenite ($TiFeO_3$). Comptes Rendus de l'Académie des Sciences de Paris, 242, 2124–2127.

Bozorth, R.M., Walsh, D.E., and Williams, A.J. (1957) Magnetization of ilmenite-hematite system at low temperatures. Physical Review, 108, 157–158.

Burton, B.P., and Davidson, P.M. (1988) Multicritical phase relations in minerals. In S. Ghose, J.M.D. Coey, and E. Salje, Eds., Structural and magnetic phase transitions in minerals, p. 60–90. Springer-Verlag, New York.

Cohen, E.R., and Taylor, B.N. (1990) The fundamental physical constants. Physics Today, 43, 9–13.

Dzyaloshinsky, I.E. (1958) A thermodynamic theory of "weak" ferromagnetism of antiferromagnetics. Journal of Physics and Chemistry of Solids, 4, 241–255.

Fritz, S.F., and Popp, R.K. (1985) A single-dissolution technique for determining FeO and Fe_2O_3 in rock and mineral samples. American Mineralogist, 70, 961–968.

Hoffman, K.A. (1975) Cation diffusion processes and self-reversal of thermoremanent magnetization in the ilmenite-hematite solid solution series. Geophysical Journal of the Royal Astronomical Society, 41, 65–80.

Huebner, J.S. (1987) Use of gas mixtures at low pressure to specify oxygen and other fugacities of furnace atmospheres. In G.C. Ulmer and H.L. Barnes, Eds., Hydrothermal experimental techniques, p. 20–60. Wiley, New York.

Ishikawa, Y. (1958a) Electrical properties of $FeTiO_3$-Fe_2O_3 solid solution series. Journal of the Physical Society of Japan, 13, 37–42.

——— (1958b) An order-disorder transformation phenomenon in the $FeTiO_3$-Fe_2O_3 solid solution series. Journal of the Physical Society of Japan, 13, 828–837.

——— (1962) Magnetic properties of ilmenite-hematite system at low temperature. Journal of the Physical Society of Japan, 17, 1835–1844.

Ishikawa, Y., and Akimoto, S. (1957) Magnetic properties of the $FeTiO_3$-Fe_2O_3 solid solution series. Journal of the Physical Society of Japan, 12, 1083–1098.

Ishikawa, Y., and Syono, Y. (1963) Order-disorder transformation and reverse thermoremanent magnetism in the $FeTiO_3$-Fe_2O_3 system. Journal of Physics and Chemistry of Solids, 24, 517–528.

Ishikawa, Y., Arai, M., Saito, N., and Kohgi, M. (1983) Spin glass properties and magnetic correlation in $FeTiO_3$-Fe_2O_3 system. Journal of Magnetism and Magnetic Materials, 31–34, 1381–1383.

Ishikawa, Y., Saito, N., Arai, M., Watanabe, Y., and Takei, H. (1985) A new oxide spin glass system of $(1 - x)FeTiO_3$-xFe_2O_3. I. Magnetic properties. Journal of the Physical Society of Japan, 54, 312–325.

Lawson, C.A., Nord, G.L., Jr., Dowty, E., and Hargraves, R.B. (1981) Antiphase domains and reverse thermoremanent magnetism in ilmenite-hematite minerals. Science, 213, 1372–1374.

Lindsley, D.H. (1965) Iron-titanium oxides. Carnegie Institution of Washington Year Book, 64, 144–148.

——— (1976a) The crystal chemistry and structure of oxide minerals as exemplified by the Fe-Ti oxides. In Mineralogical Society of America Reviews in Mineralogy, 3, L1–L60.

——— (1976b) Experimental studies of oxide minerals. In Mineralogical Society of America Reviews in Mineralogy, 3, L61–L88.

Merrill, R. (1968) A possible source for the coercivity of ilmenite-hematite minerals. Journal of Geomagnetism and Geoelectricity, 20, 181–185.

Morrish, A.H. (1965) The physical principles of rock magnetism, 680 p. Wiley, New York.

Nagata, T., and Akimoto, S. (1956) Magnetic properties of ferromagnetic ilmenites. Geofisica Pura E Applicata, 34, 36–50.

Nord, G.L., Jr., and Lawson, C.A. (1988) Order-disorder transition in Fe_2O_3-$FeTiO_3$: Structure and migration kinetics of transformation-induced twin domain boundaries. In G.W. Lorimer, Ed., Phase transformations '87, p. 576–580. Institute of Metals, London.

——— (1989) Order-disorder transition-induced twin domains and magnetic properties in ilmenite-hematite. American Mineralogist, 74, 160–176.

——— (1992) Magnetic properties of $ilmenite_{70}$-$hematite_{30}$: Effect of transformation-induced twin boundaries. Journal of Geophysical Research, 97, 10897–10910.

Salje, E.K.H., Wruck, B., and Thomas, H. (1991) Order-parameter saturation and low temperature extension of Landau theory. Zeitschrift für Physik B—Condensed Matter, 82, 399–404.

Shirane, G., Pickart, S.J., Nathans, R., and Ishikawa, Y. (1959) Neutron-diffraction study of antiferromagnetic $FeTiO_3$ and its solid solutions with α-Fe_2O_3. Journal of Physics and Chemistry of Solids, 10, 35–43.

Shirane, G., Cox, D.E., Takei, W.J., and Ruby, S.L. (1962) A study of the magnetic properties of the $FeTiO_3$-α-Fe_2O_3 system by neutron diffraction and the Mössbauer effect. Journal of the Physical Society of Japan, 17, 1598–1611.

Shomate, C.H. (1946) Heat capacity at low temperatures of the metatitanates of iron, calcium and magnesium. Journal of the American Chemical Society, 68, 964–966.

Thompson, R., and Oldfield, F. (1986) Environmental magnetism, 227 p. Allen & Unwin, Boston, Massachusetts.

Vaughan, D. (1983) Energy-dispersive X-ray microanalysis, 52 p. Kevex, Foster City, California.

Warner, B.N., Shive, P.N., Allen, J.L., and Terry, C. (1972) A study of the hematite-ilmenite series by the Mössbauer effect. Journal of Geomagnetism and Geoelectricity, 24, 353–367.

Wechsler, B.A., and Prewitt, C.T. (1984) Crystal structure of ilmenite ($FeTiO_3$) at high temperature and at high pressure. American Mineralogist, 69, 176–185.

Manuscript received September 24, 1992
Manuscript accepted May 16, 1993